Supercoiling DNA optically

Graeme A. King[a,b,1,2], Federica Burla[a,b,3], Erwin J. G. Peterman[a,b,1,4], and Gijs J. L. Wuite[a,b,1,4]

[a]Department of Physics and Astronomy, Vrije Universiteit Amsterdam, 1081 HV Amsterdam, The Netherlands; and [b]LaserLaB Amsterdam, Vrije Universiteit Amsterdam, 1081 HV Amsterdam, The Netherlands

Edited by Taekjip Ha, Johns Hopkins University, Baltimore, MD, and approved October 17, 2019 (received for review May 28, 2019)

Cellular DNA is regularly subject to torsional stress during genomic processes, such as transcription and replication, resulting in a range of supercoiled DNA structures. For this reason, methods to prepare and study supercoiled DNA at the single-molecule level are widely used, including magnetic, angular-optical, micropipette, and magneto-optical tweezers. However, it is currently challenging to combine DNA supercoiling control with spatial manipulation and fluorescence microscopy. This limits the ability to study complex and dynamic interactions of supercoiled DNA. Here we present a single-molecule assay that can rapidly and controllably generate negatively supercoiled DNA using a standard dual-trap optical tweezers instrument. This method, termed Optical DNA Supercoiling (ODS), uniquely combines the ability to study supercoiled DNA using force spectroscopy, fluorescence imaging of the whole DNA, and rapid buffer exchange. The technique can be used to generate a wide range of supercoiled states, with between <5 and 70% lower helical twist than nonsupercoiled DNA. Highlighting the versatility of ODS, we reveal previously unobserved effects of ionic strength and sequence on the structural state of underwound DNA. Next, we demonstrate that ODS can be used to directly visualize and quantify protein dynamics on supercoiled DNA. We show that the diffusion of the mitochondrial transcription factor TFAM can be significantly hindered by local regions of underwound DNA. This finding suggests a mechanism by which supercoiling could regulate mitochondrial transcription in vivo. Taken together, we propose that ODS represents a powerful method to study both the biophysical properties and biological interactions of negatively supercoiled DNA.

DNA supercoiling | optical tweezers | fluorescence microscopy | DNA–protein interactions

Torsional stress plays a vital role in many genomic processes, where it facilitates local changes in DNA topology. In order to access genetic information during transcription and replication, for example, the DNA double helix is actively unwound through the dynamic motion of translocases, such as polymerases and helicases (1–3). Torsional stress is also important for DNA compaction as it facilitates the interaction of DNA with architectural proteins such as HU and HNS in prokaryotes and histone proteins in eukaryotes (2, 4, 5). The topology of DNA is defined by its linking number (Lk), which is a linear combination of the molecular twist (Tw) and writhe (Wr). A change in DNA topology as a result of torsional stress is known as supercoiling (σ), and is quantified as the fractional change in Lk, i.e., $(Lk\text{-}Lk_0)/Lk_0$. Supercoiling can be either positive ($\sigma > 0$) or negative ($\sigma < 0$) depending on the direction of the applied torque. While both positive and negative supercoiling occur frequently in vivo, overall the genome of prokaryotes and eukaryotes is slightly negatively supercoiled (2, 4). The topological state of DNA is maintained in vivo through the action of enzymes such as topoisomerases that can relax supercoiling (6, 7). At very low DNA tensions (<1 pN), torsional stress is predominantly absorbed as writhe, yielding buckled structures known as plectonemes (8–10). At slightly higher tensions (>1 pN), negative supercoiling can induce a range of underwound DNA conformations (10–13).

The ability to study the influence of supercoiling on DNA–protein interactions is therefore of great importance. For this reason, methods to prepare and study supercoiled DNA at the single-molecule level, such as magnetic (10, 12, 14), angular-optical (13, 15, 16), micropipette (17), and magneto-optical tweezers (18, 19), are widely used. These techniques enable control of both tension and supercoiling within single molecules of DNA and have provided great insight into the mechanical action of topology-altering proteins such as helicases and topoisomerases (9, 10). In order to understand the wider role of supercoiling in genomic processes, it is vital to also consider how DNA topology alters the local interactions and spatial dynamics of DNA-binding proteins (8, 11, 20). These features are most easily identified using fluorescence imaging to correlate the presence of specific structures within the DNA molecule with the binding of fluorescently labeled proteins. However, despite recent technical advancements (8, 11, 21–23), it remains challenging to combine DNA supercoiling control with fluorescence imaging of the whole DNA molecule (9, 10, 20). Moreover, current techniques to manipulate supercoiled DNA rely on surface tethering, limiting their ability to rapidly exchange the DNA molecule between different

Significance

Torsional stress plays a vital role in many genomic transactions, including replication and transcription, and often results in underwound (negatively supercoiled) DNA. Here, we present a single-molecule method, termed Optical DNA Supercoiling (ODS), that advances our ability to study negatively supercoiled DNA. Since ODS is based on dual-trap optical tweezers, it is compatible with a wide range of functionalities that are difficult to combine with traditional methods of DNA twist control. This includes the ability to image supercoiled DNA with fluorescence microscopy and move the supercoiled substrate rapidly between different buffer/protein solutions. We demonstrate that ODS yields unique and important insights into both the biomechanical properties of negatively supercoiled DNA and the dynamics of DNA–protein interactions on underwound DNA.

Author contributions: G.A.K., E.J.G.P., and G.J.L.W. designed research; G.A.K. and F.B. performed research; G.A.K., F.B., E.J.G.P., and G.J.L.W. analyzed data; and G.A.K., F.B., E.J.G.P., and G.J.L.W. wrote the paper.

Competing interest statement: The combined optical tweezers and fluorescence technologies used in this article are patented and licensed to LUMICKS B.V., in which E.J.G.P. and G.J.L.W. have a financial interest.

This article is a PNAS Direct Submission.

Data deposition: All data associated with the manuscript and supporting information are provided in Datasets S1–S5.

[1]To whom correspondence may be addressed. Email: g.king@ucl.ac.uk, e.j.g.peterman@vu.nl, or g.j.l.wuite@vu.nl.

[2]Present address: Institute of Structural and Molecular Biology, University College London, London, WC1E 6BT, United Kingdom.

[3]Present address: Department of Living Matter, AMOLF, 1098 XG Amsterdam, The Netherlands.

[4]E.J.G.P. and G.J.L.W. contributed equally to this work.

This article contains supporting information online at https://www.pnas.org/lookup/suppl/doi:10.1073/pnas.1908826116/-/DCSupplemental.

First published December 5, 2019.

buffer and/or protein solutions. This can hinder the study of complex biological processes involving sequential protein-binding reactions.

Here, we present a multifunctional nanomechanical assay, termed Optical DNA Supercoiling (ODS), that can rapidly and controllably generate negatively supercoiled DNA using a standard dual-trap optical tweezers instrument. Supercoiled DNA formed in this way is amenable to rapid buffer exchange, and can be interrogated with both force spectroscopy and fluorescence imaging of the whole DNA. We demonstrate that this approach can provide detailed insight into the local topology of underwound DNA as well as track the spatial dynamics of proteins such as transcription factors on underwound DNA. We therefore propose that this method represents a powerful assay to study the role of DNA topology in complex and dynamic genomic processes.

Results

Generation of Negatively Supercoiled DNA Using Dual-Trap Optical Tweezers. Our method exploits the intrinsic mechanical properties of DNA to induce a fixed reduction in *Lk* (Fig. 1*A*). Here, an end-closed DNA molecule is first rendered torsionally constrained (i.e., *Lk* is fixed) through the binding of at least 2 biotin moieties (on each end of the DNA) to streptavidin-coated, optically trapped beads (24). Application of high tension (~115 pN) induces overstretching, resulting in ~70% elongation of the DNA length without any global change in *Lk* (24, 25). In the absence of torsional constraint, however, overstretching occurs at much lower forces (~65 pN) (26, 27), and is associated with cooperative unwinding of the double helix; in this case, the average molecular twist is reduced from ~10.5 bp per turn to ~37.5 bp per turn (25). Consequently, when torsionally constrained DNA is overstretched, the molecule experiences torsional stress, relative to the unconstrained state. This torsional stress can be, at least partly, released through swiveling of the DNA around a single biotin–streptavidin tether, which can happen for example when one of the biotin–streptavidin connections is disrupted (Fig. 1*B*). If the disrupted tether subsequently reforms, torsional constraint will be reinstated, but now with the DNA in a lower *Lk* than that of the B-form double helix (Fig. 1*A*). Crucially, the reduced *Lk* is preserved upon decreasing the tension (i.e., the DNA remains negatively supercoiled).

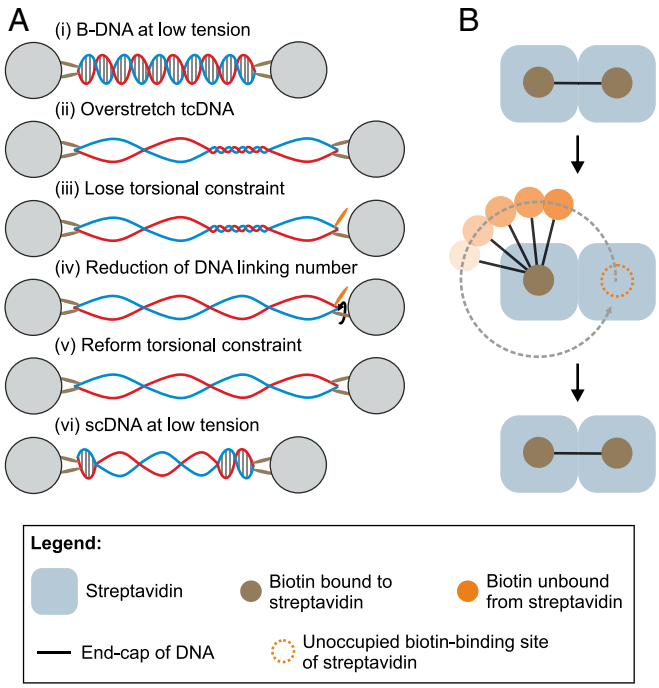

Fig. 1. Generation of negatively supercoiled DNA using dual-trap optical tweezers. (*A*, *i*) End-closed DNA is torsionally constrained between 2 optically trapped beads via at least 2 biotin–streptavidin bonds (brown ellipses) on each end of the molecule. (*A*, *ii*) The torsionally constrained DNA molecule (tcDNA) is overstretched via displacement of 1 of the beads, resulting in both overwound and underwound DNA structures (25). (*A*, *iii*) At high force (at least ~80 pN), a sufficient number of biotin–streptavidin bonds break (orange ellipse) such that only a single tether is present on at least 1 end of the DNA molecule. This results in the loss of torsional constraint. (*A*, *iv*) The DNA molecule unwinds by swiveling around the single tether (arrow). (*A*, *v*) Once the linking number has decreased, the broken biotin–streptavidin bond(s) can reform. The molecule is once again torsionally constrained, but now in a lower linking number than that of B-DNA. (*A*, *vi*) The tension is released by reducing the DNA extension, stabilizing the negatively supercoiled (sc) state. (*B*) Schematic illustration of the tethering geometry that results in the formation of constrained underwound DNA. One biotin moiety (attached to the endcap of DNA) transiently unbinds from streptavidin at high force, during which time a second biotin remains bound to another streptavidin unit. The dashed gray arrow represents DNA unwinding during the time that the biotin–streptavidin bond is disrupted.

This process is demonstrated experimentally in Fig. 2*A*. Here, we present a sample force–distance curve of highly negatively supercoiled DNA obtained using ODS (i.e., following overstretching of end-closed torsionally constrained DNA). For comparison, the force–distance curves of both unconstrained DNA and nonsupercoiled torsionally constrained DNA are shown in black and blue, respectively. The magnitude of σ can be calculated with reference to the known force–extension curves of negatively supercoiled DNA (Fig. 2*B* and *Methods*) (25). Note that the maximum error in the absolute value of σ determined using this calibration procedure is typically between 0.03 and 0.045 (*SI Appendix*, Fig. S1 and SI Note 1). The maximum value of σ that can be generated using ODS is ~−0.7: the same as that associated with fully overstretched unconstrained DNA (25). This value of σ will occur if the torsional stress is fully released by transient disruption of a biotin–streptavidin tether at high force, resulting in the red force–distance curve in Fig. 2*A*.

Importantly, the probability and timescale for tether disruption can be tuned by holding the torsionally constrained DNA molecule at high tension for different periods of time. For example, Fig. 2*C* compares sequential force–distance curves of the same DNA molecule, obtained using ODS, where after each extension the DNA molecule is held at ~150 pN for 10 s prior to retraction. The most likely value of σ generated upon retraction is typically between 0 and −0.15 (Fig. 2*D*). However, as demonstrated in Fig. 2*C*, by repeating such stretch–release cycles with the same DNA molecule, the value of σ can be tuned over a much wider range (up to $\sigma \sim -0.7$). The above behavior accounts for ~25% of cases, where supercoiling is only generated at forces >115 pN (i.e., beyond the end of the overstretching transition). In another 25–35% of molecules, one of the biotin–streptavidin tethers is even less stable, and will already transiently disrupt during overstretching—this allows the magnitude of σ to be even more precisely controlled, simply by tuning the extent to which the molecule is initially overstretched (Fig. 2 *E* and *F*). A summary of the various force–distance behaviors of end-capped torsionally constrained DNA is provided in *SI Appendix*, Figs. S2 and S3 and SI Note 2.

ODS Yields a Stable Change in DNA Linking Number. The ability of ODS to produce and maintain a reduced DNA linking number relies on 2 assumptions. The first is that the supercoiling generated is not easily dissipated through free rotation of the optically trapped beads. It has previously been reported that for supercoiled DNA in the range of $-0.1 > \sigma > -1.5$, the torque is roughly constant at approximately −10 pN nm (11, 13). The rotational velocity of the beads in response to such an applied torque is inversely proportional to the cube of the bead radius and can be calculated using the equations of rotational motion (*SI Appendix*, SI Note 3). From these equations, the timescale for a single bead

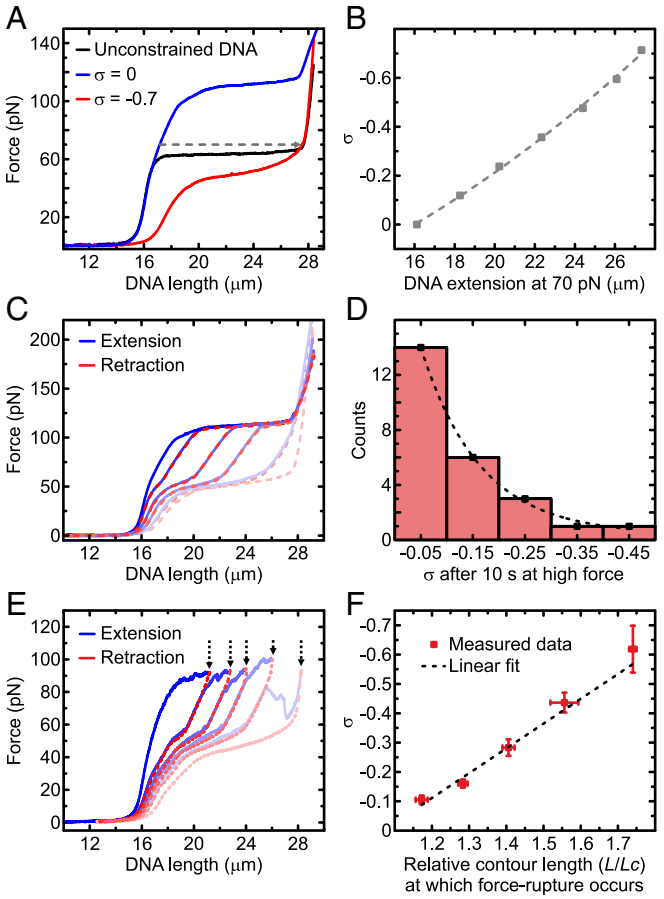

Fig. 2. Controlling the extent of supercoiling obtained using ODS. (*A*) Sample force–distance curve of negatively supercoiled DNA (σ = −0.7, red) obtained using ODS. For comparison, the force–distance curves of torsionally unconstrained DNA (black) and torsionally constrained DNA (σ = 0, blue) are also shown. The dashed gray line highlights the change in length between supercoiled and nonsupercoiled DNA at 70 pN used for calibration. (*B*) Reference plot showing the change in σ as a function of DNA extension at 70 pN, as determined from previously published force–extension curves of supercoiled DNA (25). These data are interpolated using a second-order polynomial (dashed gray line). Data from ref. 25. (*C*) In a subset of molecules (~25%), the magnitude of σ can be controlled by repeatedly extending the molecule (blue) and waiting at high forces (>115 pN) for a given period of time. Force–distance curves associated with repeated stretch/relax cycles are shown by the fading blue/red color scheme. The force–retraction curves (dashed red) obtained following each extension are consistent with increasing magnitudes of σ (25). (*D*) Histogram showing that, for the subset of molecules that behave similar to those in *C*, the average value of σ generated after 10 s at ~150 pN is ~−0.1 (n = 25). However, much larger magnitudes of σ (up to ~−0.7) can be generated easily by repeating the above procedure several times (as shown by the force–distance curves in *C*). (*E*) In another subset of molecules (~25 to 35%), the supercoiled state is generated following force ruptures that occur between 80 and 120 pN (blue). After each force rupture (black arrows), an increasing magnitude of σ is formed (as evidenced by the force–retraction curves, dashed red). (*F*) For the behavior described in *E*, the average value of σ formed is roughly proportional to the extension at which the force rupture occurred (n = 15). All errors are SEM.

rotation is calculated to be ~180 s when using 4.5-μm-diameter beads. Moreover, the timescale for converting the entire molecule from a supercoiled state to a nonsupercoiled state depends on the total number of base pairs in the molecule. Assuming a torque of −10 pN nm and 4.5-μm-diameter beads, it should take ~170 h to fully convert a λ-DNA molecule (48,502 bp) from a highly supercoiled state (σ ~ −0.7) to a nonsupercoiled state through rotational motion of the beads (Fig. 3*A*, dark blue). The fractional change in *Lk* over time also depends on the initial value of σ, as highlighted in Fig. 3*A* (shaded blue). Nevertheless, Fig. 3*A* indicates that, assuming long DNA and large beads are used, the total change in *Lk* due to bead rotation is negligible on the timescale of most single-molecule experiments. Additionally, any small asymmetries in the shape of the beads will likely result in a preferred orientation in the optical traps, and thus further hinder rotational motion.

The second key assumption underpinning ODS is that the biotin–streptavidin bonds are stable at low forces: any transient loss of torsional constraint due to cleavage of a tether could lead to rewinding of the double helix and loss of supercoiling. Indeed, it is the transient cleavage of a biotin–streptavidin tether that is the basis of ODS. However, such cleavage is promoted by tension; it has been predicted previously that the lifetime of a biotin–streptavidin bond is several orders of magnitude lower at forces >100 pN than at forces <10 pN (28).

To test the above assertions experimentally, we measured the change in *Lk* (and thus σ) over time by monitoring the DNA extension at a fixed force (5, 20, and 40 pN, respectively). At these tensions, negatively supercoiled DNA (for σ in the range of −0.1 to −0.7) is longer than B-form DNA, and thus any change in σ should be detected through a change in extension (*SI Appendix*, Fig. S4). In a small subset of cases (10%, n = 3/30) a clear change in σ was observed within a 10-min time span. However, for the vast majority of molecules considered (90%, n = 27/30), negligible change in extension (and thus σ) was detected over a 30-min period. We note that the few molecules that are unstable typically lose their supercoiled state within a short period of time and can therefore be easily identified and screened for.

Unraveling the Structure of Negatively Supercoiled DNA Using ODS. To demonstrate the power of ODS, we first apply this method to study the structural and mechanical properties of underwound DNA as a function of ionic strength and tension. The structural transitions of negatively supercoiled DNA are of particular interest as a result of their role in both transcription and replication (1–3, 9, 10). It has been reported previously that upon changing σ from −0.1 to −1.5, torsionally constrained DNA held at ~5 pN undergoes a cooperative transition from B-DNA to an increasingly underwound state (11–13). The underwound regions have been reported to exist as several different structures, including left-handed conformations (L-DNA and Z-DNA) as well as less defined base-pair melted conformations (bubble-melted DNA) (11). However, the exact structures of underwound DNA and their

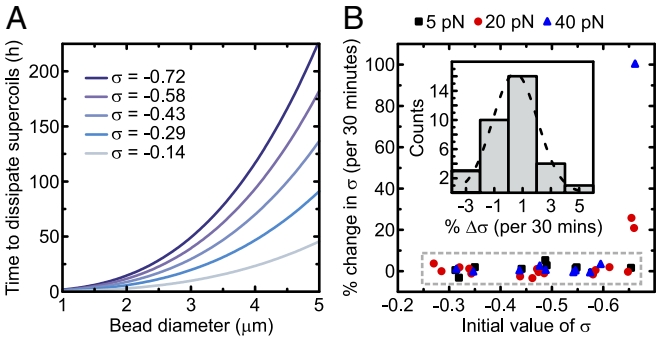

Fig. 3. The reduced linking number generated via ODS is constant over time at forces ≤ 40 pN. (*A*) Predicted timescale for complete rewinding of negatively supercoiled DNA due to bead rotation as a function of bead diameter. This is shown here for a λ-DNA molecule (48,502 bp) with different initial extents of supercoiling (−0.14 > σ > −0.72). The calculations are based on the standard equations of rotational motion (*SI Appendix*, SI Note 3). (*B*) Experimentally determined fractional change in σ over 30 min for supercoiled DNA held at a constant force (5, 20, or 40 pN). (*Inset*) Histogram showing the change in σ for the data contained within the gray dashed box.

dependence on local (e.g., cellular) environment are unclear. To gain a better understanding of this, we recorded force–extension curves of negatively supercoiled DNA as a function of ionic strength (Fig. 4 *A* and *B*). These experiments reveal 2 notable features. The first is that, for NaCl concentrations below ∼50 mM, the overstretching transition appears less cooperative (i.e., the change in force as a function of extension is more gradual and less smooth). Second, at very low ionic strength (<25 mM NaCl) hysteresis is observed when comparing force–extension and force–retraction curves (Fig. 4*B*). A similar hysteresis is also induced at elevated temperature (*SI Appendix*, Fig. S5). These observations indicate that underwound DNA exhibits a heterogeneous structure, and is at least partially base-pair melted at low ionic strength. By fitting the extensible worm-like chain model (up to 30 pN) to the force–extension curves of supercoiled DNA, quantitative information can be extracted (Fig. 4*C* and *SI Appendix*, Fig. S6). These fits reveal a significant decrease in the apparent DNA persistence length, from ∼57 to ∼30 nm as σ is varied from −0.08 to −0.65. Concomitant with this, the apparent DNA contour length increases by ∼8% over the same range of σ. This is consistent with the presence of both L-DNA and bubble-melted DNA, which have each been reported to exhibit a lower persistence length and a greater contour length than B-DNA (13).

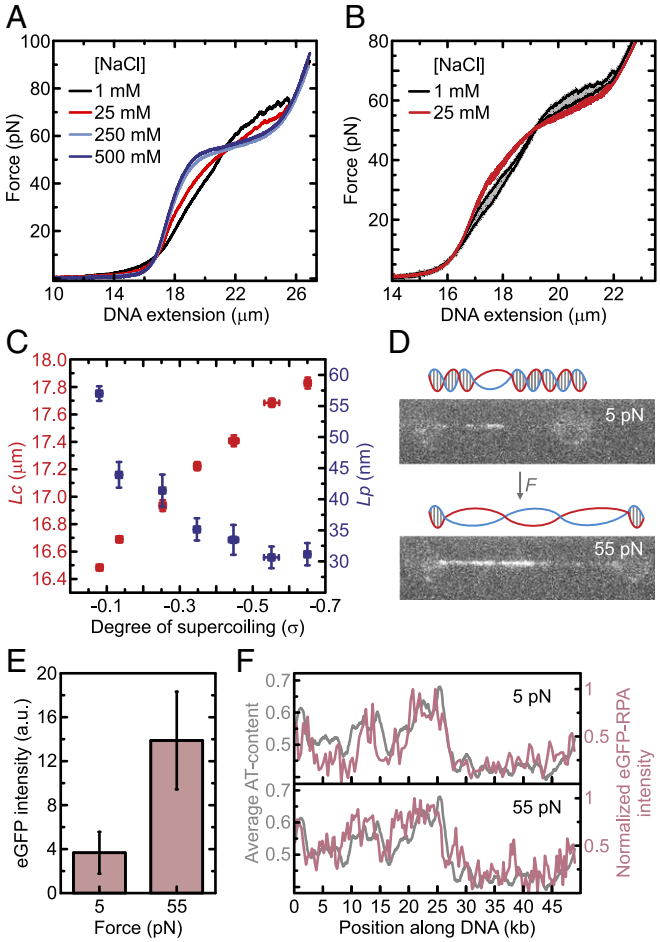

Fig. 4. Application of ODS to study the structural and mechanical properties of underwound DNA. (*A*) Force–extension curves of negatively supercoiled DNA (σ = −0.55) recorded in a range of NaCl concentrations (1 to 500 mM). (*B*) Comparison of force–extension and force–retraction curves of negatively supercoiled DNA (σ = −0.34) in 1 mM NaCl and 25 mM NaCl, respectively. Filled gray areas highlight the observed hysteresis. (*C*) Contour length (*Lc*) and persistence length (*Lp*) of DNA as a function of σ determined from fits of the extensible worm-like chain model to experimentally derived force–distance curves (up to 30 pN) at 25 mM NaCl. Note that the DNA is expected to consist of regions of both B-DNA and underwound structures (such as L-DNA). Thus, the measured *Lc* and *Lp* are average values for the entire DNA molecule, rather than for 1 specific structure. (*D*) Sample fluorescence images for eGFP-RPA bound to negatively supercoiled DNA (σ = −0.59) at 5 and 55 pN, respectively. Images were recorded in the presence of the protein (0.8 nM) after incubation for 2 min. (*E*) Comparison of the average fluorescence intensity of eGFP-RPA bound to negatively supercoiled DNA at 5 pN (σ = −0.69 ± 0.04, $n = 4$) and 55 pN (σ = −0.67 ± 0.03, $n = 4$). The errors in σ represent the spread of σ values within each dataset. (*F*) Comparison of the eGFP-RPA fluorescence intensity with the average AT content along the length of the DNA molecule (at both 5 and 55 pN). Unless specified otherwise, the buffer contained 25 mM NaCl. Errors are SEM.

To gain more insight into the structure of underwound DNA, we imaged the binding of fluorescently labeled replication protein A (eGFP-RPA) to negatively supercoiled DNA. This protein has previously been used to identify bubble-melted domains of DNA under mechanical strain (11, 24, 26). We first confirm that at low concentrations (0.8 nM), RPA does not significantly perturb the structure of underwound DNA (*SI Appendix*, Fig. S7 and SI Note 4). Next, we compare the binding of eGFP-RPA to negatively supercoiled DNA at 5 and 55 pN, respectively (for σ between −0.6 and −0.7). Note that the binding affinity of RPA for base-pair melted DNA is tension independent (26). These experiments were performed by incubating the DNA molecule in RPA (0.8 nM) for 2 min and then recording a snapshot image (e.g., Fig. 4*D*). The images reveal 3 important observations. The first is that eGFP-RPA binding is observed at low forces (∼5 pN). This suggests that, at low tensions, localized regions of the DNA are base-pair melted and sufficiently accessible for RPA (which has a footprint of ∼30 nucleotides (26)). This observation is consistent with recent studies of RPA binding by Vlijm et al. (*SI Appendix*, SI Note 5) (11). The second key finding is that a significant (∼3–4-fold) increase in RPA binding to negatively supercoiled DNA is observed at 55 pN, compared with 5 pN (Fig. 4 *D* and *E* and *SI Appendix*, Fig. S8), indicating that force assists the further melting of the DNA. Third, eGFP-RPA binding (at both low and high forces) is observed primarily in the most AT-rich domains of the DNA molecule (Fig. 4*F*). Such sequences have been shown previously to promote base-pair melting under mechanical stress (24, 26). Together, the above findings support a growing body of evidence that negatively supercoiled DNA exhibits a heterogeneous structure at low forces (e.g., 5 pN) and low salt concentrations (e.g., 25 mM NaCl), with a coexistence of at least L-DNA, B-DNA, and bubble-melted structures (11–14).

ODS Reveals Topology-Dependent Transcription Factor Diffusion. Given the ability of ODS to combine supercoiled DNA manipulation with both wide-field fluorescence imaging and rapid buffer exchange, the method is well-suited to probe protein dynamics on supercoiled DNA. To demonstrate this, we investigate how negative supercoiling can influence the diffusion of the mitochondrial transcription factor TFAM (Mitochondrial Transcription Factor A). This protein has vital roles in transcription initiation, replication, and transmission of mitochondrial DNA (29, 30). TFAM has been shown previously to diffuse rapidly on B-form DNA via a 1D sliding motion, with a diffusion coefficient of $\sim 10 \times 10^4$ nm^2 s^{-1} (30). It has been proposed that this sliding provides a mechanism for the protein to efficiently search for its promoter sites on the mitochondrial genome (30). Notably, the mitochondrial genome is circular (and therefore torsionally constrained) and is believed to exhibit a range of topologies in vivo, including negatively supercoiled states (31). However, the influence of supercoiling on TFAM diffusion and on protein diffusion in general is unknown. To address this, we used ODS to compare the dynamics of TFAM on a range of underwound and nonsupercoiled DNA substrates (Fig. 5*A*). Here, we incubated each DNA substrate in a low concentration of TFAM (fluorescently labeled with Alexa Fluor 555). Each DNA substrate was subsequently moved to a protein-free

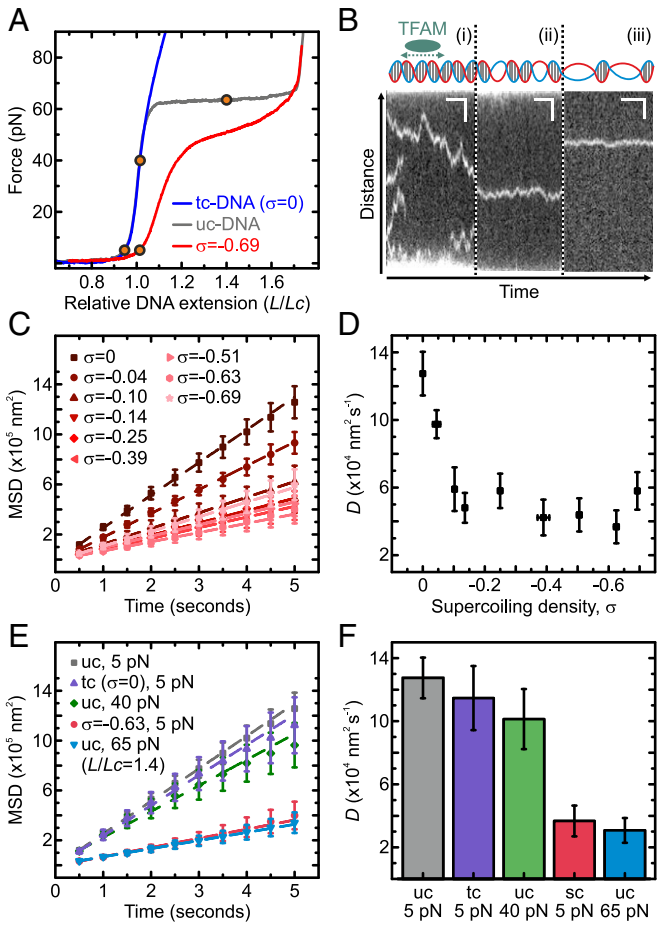

Fig. 5. Application of ODS to study TFAM diffusion on underwound DNA. (*A*) Sample force–extension curves of end-closed torsionally unconstrained (uc) DNA (gray), torsionally constrained (tc) DNA (σ = 0, blue) and negatively supercoiled (sc) DNA (σ = −0.69, red). Orange circles indicate the forces/extensions at which TFAM diffusion was studied. (*B*) Sample kymographs for Alexa-555-TFAM monomers on (*B, i*) B-DNA at 5 pN, (*B, ii*) sc-DNA (σ = −0.69) at 5 pN, and (*B, iii*) overstretched uc-DNA with relative extension *L*/*Lc* = 1.4 (~65 pN). (Scale bars, 2 μm and 10 s, respectively.) The schematic illustrates TFAM diffusion on (*B, i*) B-DNA, (*B, ii*) sc-DNA, with small bubble-melted regions, and (*B, iii*) overstretched DNA, with extended bubble-melted structures. (*C*) MSD of Alexa-555-TFAM monomers as a function of time on uc-DNA (σ = 0) and sc-DNA (−0.04 > σ > −0.69) at 5 pN. Dashed lines indicate linear fits to the data. (*D*) Diffusion coefficients (*D*) for TFAM monomers as a function of supercoiling density (0 ≥ σ ≥ −0.69) at 5 pN, extracted from the fits to the data in *C*. (*E*) MSD of TFAM monomers as a function of time on uc-DNA at 5 pN (gray), tc-DNA (σ = 0) at 5 pN (purple), uc-DNA at 40 pN (green), sc-DNA (σ = −0.63) at 5 pN (red), and overstretched uc-DNA at *L*/*Lc* = 1.4 (~65 pN, blue), respectively. Dashed lines indicate linear fits to the data. (*F*) Diffusion coefficients for monomers of TFAM on the substrates in *E*, extracted from the fits to the data in *E*. Data in *C*–*F* were derived from analysis of >10 TFAM monomers for each DNA substrate. Data in *C* and *D* were binned according to similar values of σ (*SI Appendix*, SI Note 6). All errors are SEM.

buffer channel allowing the imaging of monomers of Alexa-555-TFAM bound to the DNA (Fig. 5*B*). Using single-particle tracking, we then calculated the average mean-squared displacement (MSD) of TFAM monomers on each DNA substrate over time.

We first examined the influence of negative supercoiling on TFAM diffusion at low DNA tensions (5 pN). As shown in Fig. 5*C*, the MSD of TFAM increases linearly with time in all cases, consistent with free 1D diffusion. However, the diffusion coefficient for TFAM (determined from the slopes in Fig. 5*C*) decreases significantly as a function of negative supercoiling. As summarized in Fig. 5*D*, the diffusion coefficient for TFAM on DNA at 5 pN decreases by up to ~65% as σ is varied from 0 to −0.69. Interestingly, a substantial decrease in diffusion requires only a relatively modest superhelical density (σ ~ −0.15). Since negatively supercoiled DNA contains small regions of base-pair melted DNA at 5 pN (Fig. 4 and *SI Appendix*), we hypothesize that these bubbles reduce the mobility of the protein. To confirm this, we next measured the diffusion of TFAM on overstretched end-closed unconstrained DNA, which contains extended bubble-melted structures at low ionic strength. Analysis of the corresponding MSD behavior (Fig. 5*E*, blue) reveals that TFAM diffusion is similar, or even slightly slower, on overstretched unconstrained DNA compared with negatively supercoiled DNA at 5 pN (Fig. 5*F*). As controls, we note that TFAM diffusion on nonsupercoiled DNA at 5 pN is unaffected by the presence of torsional constraint and is only minimally force dependent (Fig. 5 *E* and *F*). Together, these observations indicate that TFAM mobility on DNA is highly sensitive to the presence of underwound structures—either due to negative supercoiling or overstretching.

While the mobility of TFAM on nonsupercoiled (B-form) DNA is rapid, it is still lower than the maximum limit for rotation-coupled diffusion along the DNA backbone (32). This implies that the protein is slowed down by more stable transient interactions with the DNA. The current work suggests that these interactions are either stronger and/or less transient when the DNA is underwound. This is consistent with a recent study showing that TFAM has a higher binding affinity for negatively supercoiled plasmids (33). We thus propose that TFAM interacts more strongly with local underwound structures, resulting in a slower 1D sliding on DNA. It is notable that, despite the reduced diffusion of TFAM on underwound structures, we do not observe evidence of confined diffusion on these substrates (Fig. 5 *C* and *E*). Therefore, although underwound DNA structures can reduce TFAM diffusion, the protein is still capable of sliding over such structures. Taken together, this has potentially important implications for the ability of TFAM to locate and interact with promoter sites in vivo and suggests a mechanism by which supercoiling could regulate processes such as mitochondrial transcription.

Discussion

Here we have presented a versatile methodology to generate and study negatively supercoiled DNA at the single-molecule level. Since ODS is based on a standard dual-trap optical tweezers assay, it is compatible with a wide range of functionalities that are difficult to combine with traditional methods to control DNA linking number. Importantly, this includes the ability to image the whole DNA molecule with fluorescence microscopy (20, 34). Additionally, the supercoiled substrate can be freely moved between different microfluidic channels, allowing for fast buffer exchange. This latter feature is greatly advantageous because it facilitates sequential binding of different proteins to the substrate, and also enables fluorescence images to be recorded under background-free conditions (20). Furthermore, in ODS, the supercoiled state is generated rapidly (on the order of seconds), independent of the length of the DNA molecule. This is important because it facilitates the use of much longer substrates (such as λ-DNA), which is beneficial for many fluorescence imaging studies (20).

Exploiting the above features, we have used ODS to quantify the heterogeneous structure of underwound DNA and reveal how these structures can influence the mobility of a key mitochondrial transcription factor. These applications showcase the unique ability of ODS to interrogate long molecules of supercoiled DNA using a combination of 3D nanomanipulation and fluorescence microscopy. In this way, we demonstrate that the method is a robust and powerful approach for probing the structural properties of underwound DNA as well as the interplay between negative supercoiling and DNA-binding proteins. We propose that ODS can therefore be applied to address many open questions in

genome biology, by enabling detailed mechanistic studies of, for example, RNA polymerases, helicases, and topoisomerases on supercoiled substrates. To this end, we envision that the technique could be even further functionalized through integration with, for example, Förster Resonance Energy Transfer (FRET) (34), superresolution imaging (20), and fluorescence polarization microscopy (35).

Methods

DNA Construct Design. End-closed DNA molecules (~48.5 kb) were prepared by ligating an endcap to each terminal *cos*-site of λ-DNA (24). Each endcap was composed of a 5-T loop adjoined to a 12-bp double-stranded stem and a 12-nucleotide single-stranded overhang (*SI Appendix, SI Methods*). Biotin moieties were covalently attached to 4 thymine residues within or near the 5-T loop. Once each endcap was ligated to λ-DNA, the DNA molecule could be tethered between 2 streptavidin-coated beads via biotin–streptavidin bonds. The number of biotins that bind to a given bead is variable: in the majority of cases (~90 to 95%), at least 2 biotins on each end of the DNA molecule bind to a bead. This renders the DNA molecule unable to change its total linking number and the molecule is thus torsionally constrained.

Single-Molecule Assays. We employed a custom-built inverted microscope that combines dual-trap optical tweezers and wide-field fluorescence microscopy (24, 26). Experiments were performed in a multichannel laminar flow cell where end-closed DNA was tethered between 2 microspheres (each of diameter 4.5 μm) in situ. Such a flow cell also allowed this dumbbell construct to be exchanged rapidly between channels containing different buffers or ligands. Forces applied to the DNA (via displacement of a tethered microsphere) were measured via back-focal plane interferometry of the condenser top lens using a position-sensitive detector (20). Data were obtained at room temperature in a buffer of 20 mM Tris·HCl, pH 7.6. The buffer also contained 25 mM NaCl, unless stated otherwise. eGFP-RPA and Alexa-555-TFAM were prepared as detailed previously (26, 32).

Calibrating the Extent of Supercoiling. The fixed change in DNA linking number generated using ODS can be calibrated using reference force–extension curves. Such reference curves can be obtained either from literature or independently using alternative single-molecule approaches (such as magnetic or micropipette tweezers). In our case, we chose to compare our force–extension curves with those of Léger et al (25). To this end, we plotted the DNA extension at 70 pN as a function of σ. At this force, the reference data show a near-linear relationship between the DNA extension at 70 pN and σ (over the range of $0 > \sigma > -0.7$; see Fig. 2*B*). By comparing the DNA extension from our measurements at 70 pN with those of the reference data, the value of σ generated in our method can be determined. The uncertainty in the absolute value of σ determined using this calibration procedure is typically between 0.03 and 0.045 (*SI Appendix*, Fig. S1 and SI Note 1).

TFAM Diffusion Analysis. End-closed DNA molecules were incubated in a low concentration of Alexa-555-labeled TFAM (~5 nM) such that only a few protein monomers were bound. The DNA molecules were then transferred to a protein-free buffer channel where fluorescence videos were recorded with a frame rate of 0.5 s. Kymographs of these videos were then analyzed with a custom-written MATLAB-based program that tracked the position of each Alexa-555-TFAM monomer on the DNA as a function of time. Only traces spanning longer than 10 s and which did not cross another were considered. The diffusion constant (D) was determined from MSD plots ($\mathrm{MSD} = 2Dt + \text{offset}$) for all trajectories measured.

ACKNOWLEDGMENTS. We thank Mauro Modesti (Cancer Research Center of Marseille) and Carolyn Suzuki (Rutgers New Jersey Medical School) for the kind gift of eGFP-RPA and TFAM, respectively. The authors are grateful to Andreas Biebricher for helpful discussions and Iddo Heller for providing kymograph position tracking software. The work was supported by funding through a Human Frontier Science Program grant (G.J.L.W.), Vici grants from the Netherlands Organization for Scientific Research (NWO) (G.J.L.W. and E.J.G.P.), an NWO Chemical Sciences Top grant (G.J.L.W. and E.J.G.P.) and a European Molecular Biology Organization (EMBO) long-term postdoctoral fellowship (G.A.K.).

1. F. Kouzine, S. Sanford, Z. Elisha-Feil, D. Levens, The functional response of upstream DNA to dynamic supercoiling in vivo. *Nat. Struct. Mol. Biol.* **15**, 146–154 (2008).
2. C. Naughton *et al*., Transcription forms and remodels supercoiling domains unfolding large-scale chromatin structures. *Nat. Struct. Mol. Biol.* **20**, 387–395 (2013).
3. J. Ma, L. Bai, M. D. Wang, Transcription under torsion. *Science* **340**, 1580–1583 (2013).
4. M. S. Luijsterburg, M. F. White, R. van Driel, R. T. Dame, The major architects of chromatin: Architectural proteins in bacteria, archaea and eukaryotes. *Crit. Rev. Biochem. Mol. Biol.* **43**, 393–418 (2008).
5. S. C. Dillon, C. J. Dorman, Bacterial nucleoid-associated proteins, nucleoid structure and gene expression. *Nat. Rev. Microbiol.* **8**, 185–195 (2010).
6. S. M. Vos, E. M. Tretter, B. H. Schmidt, J. M. Berger, All tangled up: How cells direct, manage and exploit topoisomerase function. *Nat. Rev. Mol. Cell Biol.* **12**, 827–841 (2011).
7. Y. Seol, K. C. Neuman, The dynamic interplay between DNA topoisomerases and DNA topology. *Biophys. Rev.* **8**, 221–231 (2016).
8. M. T. van Loenhout, M. V. de Grunt, C. Dekker, Dynamics of DNA supercoils. *Science* **338**, 94–97 (2012).
9. J. Lipfert, M. M. van Oene, M. Lee, F. Pedaci, N. H. Dekker, Torque spectroscopy for the study of rotary motion in biological systems. *Chem. Rev.* **115**, 1449–1474 (2015).
10. S. Forth, M. Y. Sheinin, J. Inman, M. D. Wang, Torque measurement at the single-molecule level. *Annu. Rev. Biophys.* **42**, 583–604 (2013).
11. R. Vlijm, A. Mashaghi, S. Bernard, M. Modesti, C. Dekker, Experimental phase diagram of negatively supercoiled DNA measured by magnetic tweezers and fluorescence. *Nanoscale* **7**, 3205–3216 (2015).
12. F. C. Oberstrass, L. E. Fernandes, Z. Bryant, Torque measurements reveal sequence-specific cooperative transitions in supercoiled DNA. *Proc. Natl. Acad. Sci. U.S.A.* **109**, 6106–6111 (2012).
13. M. Y. Sheinin, S. Forth, J. F. Marko, M. D. Wang, Underwound DNA under tension: Structure, elasticity, and sequence-dependent behaviors. *Phys. Rev. Lett.* **107**, 108102–108106 (2011).
14. Z. Bryant *et al*., Structural transitions and elasticity from torque measurements on DNA. *Nature* **424**, 338–341 (2003).
15. A. La Porta, M. D. Wang, Optical torque wrench: Angular trapping, rotation, and torque detection of quartz microparticles. *Phys. Rev. Lett.* **92**, 190801–190804 (2004).
16. C. Deufel, S. Forth, C. R. Simmons, S. Dejgosha, M. D. Wang, Nanofabricated quartz cylinders for angular trapping: DNA supercoiling torque detection. *Nat. Methods* **4**, 223–225 (2007).
17. M. Nöllmann *et al*., Multiple modes of Escherichia coli DNA gyrase activity revealed by force and torque. *Nat. Struct. Mol. Biol.* **14**, 264–271 (2007).
18. X. J. A. Janssen *et al*., Electromagnetic torque tweezers: A versatile approach for measurement of single-molecule twist and torque. *Nano Lett.* **12**, 3634–3639 (2012).
19. S. Selvam, D. Koirala, Z. Yu, H. Mao, Quantification of topological coupling between DNA superhelicity and G-quadruplex formation. *J. Am. Chem. Soc.* **136**, 13967–13970 (2014).
20. I. Heller, T. P. Hoekstra, G. A. King, E. J. G. Peterman, G. J. L. Wuite, Optical tweezers analysis of DNA-protein complexes. *Chem. Rev.* **114**, 3087–3119 (2014).
21. E. T. Graves *et al*., A dynamic DNA-repair complex observed by correlative single-molecule nanomanipulation and fluorescence. *Nat. Struct. Mol. Biol.* **22**, 452–457 (2015).
22. J. Fan, M. Leroux-Coyau, N. J. Savery, T. R. Strick, Reconstruction of bacterial transcription-coupled repair at single-molecule resolution. *Nature* **536**, 234–237 (2016).
23. Y. Seol, K. C. Neuman, Combined magnetic tweezers and micro-mirror total internal reflection fluorescence microscope for single-molecule manipulation and visualization. *Methods Mol. Biol.* **1665**, 297–316 (2018).
24. G. A. King, E. J. G. Peterman, G. J. L. Wuite, Unravelling the structural plasticity of stretched DNA under torsional constraint. *Nat. Commun.* **7**, 11810–11817 (2016).
25. J. F. Léger *et al*., Structural transitions of a twisted and stretched DNA molecule. *Phys. Rev. Lett.* **83**, 1066–1069 (1999).
26. G. A. King *et al*., Revealing the competition between peeled ssDNA, melting bubbles, and S-DNA during DNA overstretching using fluorescence microscopy. *Proc. Natl. Acad. Sci. U.S.A.* **110**, 3859–3864 (2013).
27. X. Zhang *et al*., Revealing the competition between peeled ssDNA, melting bubbles, and S-DNA during DNA overstretching by single-molecule calorimetry. *Proc. Natl. Acad. Sci. U.S.A.* **110**, 3865–3870 (2013).
28. R. Merkel, P. Nassoy, A. Leung, K. Ritchie, E. Evans, Energy landscapes of receptor-ligand bonds explored with dynamic force spectroscopy. *Nature* **397**, 50–53 (1999).
29. H. S. Hillen, Y. I. Morozov, A. Sarfallah, D. Temiakov, P. Cramer, Structural basis of mitochondrial transcription initiation. *Cell* **171**, 1072–1081.e10 (2017).
30. G. Farge *et al*., Protein sliding and DNA denaturation are essential for DNA organization by human mitochondrial transcription factor A. *Nat. Commun.* **3**, 1013 (2012).
31. J. E. Kolesar, C. Y. Wang, Y. V. Taguchi, S. H. Chou, B. A. Kaufman, Two-dimensional intact mitochondrial DNA agarose electrophoresis reveals the structural complexity of the mammalian mitochondrial genome. *Nucleic Acids Res.* **41**, e58 (2013).
32. G. A. King *et al*., Acetylation and phosphorylation of human TFAM regulate TFAM-DNA interactions via contrasting mechanisms. *Nucleic Acids Res.* **46**, 3633–3642 (2018).
33. T. R. Litwin, M. Solà, I. J. Holt, K. C. Neuman, A robust assay to measure DNA topology-dependent protein binding affinity. *Nucleic Acids Res.* **43**, e43 (2015).
34. M. J. Comstock *et al*., Protein structure. Direct observation of structure-function relationship in a nucleic acid-processing enzyme. *Science* **348**, 352–354 (2015).
35. A. S. Backer *et al*., Single-molecule polarization microscopy of DNA intercalators sheds light on the structure of S-DNA. *Sci. Adv.* **5**, v1083 (2019).